MTLA 33 (2024) 102031

Contents lists available at ScienceDirect

Materialia

journal homepage: www.elsevier.com/locate/mtla

Full Length Article

An approach to understanding the formation mechanism of $NiFe_2O_4$ inverse spinel

Oscar A. Restrepo [a,*], Óscar Arnache [b], Normand Mousseau [c]

[a] Biophysics Group, Institute of Physics, University of Antioquia 050010, Medellín, Colombia
[b] Grupo de Estado Sólido-GES, Universidad de Antioquia, A.A. 1226, Instituto de Física, Medellín, Colombia
[c] Département de physique, Institut Courtois and Regroupement québécois sur les matériaux de pointe, Université de Montréal, Case postale 6128, succursale centre-ville, Montréal (QC) H3C 3J7, Canada

ARTICLE INFO

Keywords:
Inverse spinel formation
Diffusion spinels
NiFe2O4
KMC
Mössbauer

ABSTRACT

The role of diffusion in the formation of the inverse spinel phase, as opposed to the normal phase which is never observed, is still not well understood. This is in part due to the difficulty or impossibility to do *in situ* experiments to observe how the inverse spinel phase forms, owing to the small reaction/transition times and equipment sensitivity. Here, we show that diffusion of point defects such as cation interstitials is responsible for the transition from normal to inverse spinel, which explains why a normal phase is never observed. These mechanisms are studied computationally using the kinetic activation-relaxation technique (k-ART), an off-lattice kinetic Monte Carlo algorithm. We find, in particular, how Fe and Ni kinetics both support the Ni interstitial diffusion with low activation barriers. The inverse spinel structure is analyzed by Mossbauer and XRD *ex situ* experimental results which corroborate inverse spinel formation.

1. Introduction

Spinel-ferrite $NiFe_2O_4$ is associated with several technological applications such as steel fabrication, metal corrosion oxidation, spintronics, microwave absorption, gas sensors, photocatalyst in hydrogen production, fabrication of fusion and fission reactors, etc. [1–4], hence, its relevant importance.

A spinel is described by the general formula AB_2O_4 and is categorized as normal, inverse or mixed depending on cation distribution in the tetrahedral and octahedral sites [5]. For nickel-ferrite $NiFe_2O_4$, the most chemically stable structure is the inverse spinel where Fe^{3+} atoms fill all 8 tetrahedral A-sites and Ni^{2+} and Fe^{3+} fill randomly the 16 octahedral B-sites; the normal is never observed however. This inversion is explained experimentally by the fact that the energy E necessary for a Ni^{2+} ion on a B-site to be exchanged with a Fe^{3+} ion on an A-site is ~0.8 eV, and experiments predict that, at a temperature T, the fraction x of Ni^{2+} ions on A-sites should follow the relation $x = e^{-E/K_BT}$, with $x \ll 1$, explaining the inverse spinel [6–8]. Also, due to the polycrystalline nature as a result of the synthesis process, grain boundaries may play a relevant role allowing Ni to be found in tetrahedral sites (similar to the surface on ferrite nanoparticles [9,10]). More recently, the cation distribution of a general spinel has also been explained by considering the ionization energy of the cations, the Pauli repulsion energy, the magnetic ordering energy and the tendency towards charge density balance [11,12]. Nevertheless, these theories are not able to explain the exact dynamics of inverse spinel formation, i.e., it is not well understood which mechanisms in the synthesis process are responsible for obtaining an inverse spinel rather than a normal one, and whether diffusion plays a role in spinel formation. Experimentally, it is known that the nucleation process is followed by the formation of spinel in an ordered lattice at temperatures >800°C [13], and during this process diffusion of defects as interstitials should play a relevant role in the final cation distribution x (measured in *ex situ* experiments). However, the mechanisms responsible for spinel formation after nucleation are still unknown.

From an experimental point of view there are several methods to identify the type of spinel. One of them is Mossbauer spectroscopy. However, it is difficult to understand the formation mechanisms of these types of structures in the synthesis processes (sol-gel, self-combustion, solid state reaction, mechanical ball milling, physical vapor deposition - PVD, hydrothermal method, spray pyrolysis, among others) [14]. The formation mechanisms of the samples in bulk, nanoparticles or nanostructures have led to changes in morphology, particle sizes, changes in structural parameters and physical properties, where the temperature,

* Corresponding author.
E-mail address: ores77@gmail.com (O.A. Restrepo).

https://doi.org/10.1016/j.mtla.2024.102031
Received 3 August 2023; Accepted 1 February 2024
Available online 2 February 2024

applied high-pressure, cooling process, irradiation with high-energy electrons, ions or neutrons are usually factors as responsible for the inversion degree attained by the spinels [15,16]. In order to investigate the mechanism of spinel formation process, both the rate-controlling reaction and the activation energy must be determined. In many cases the actual kinetic equations are rather complicated and the methods considered by some authors, cannot be applied without modification in the wide temperature range used in the process [13,17]. Despite all the experimental efforts to understand these formation mechanisms, a full understanding has not yet been possible because reactions at the molecular level occur on a scale inaccessible to these techniques. Due to these limitations, few studies have attempted to identify the atomic level processes by which cations diffuse through the spinel structure, but the mechanisms and related phenomena that lead to inversion type of these materials are mostly not understood. Nevertheless, in recent years some theoretical and computational studies have been reported to have a better understanding of the processes at the atomic level where diffusion and vacancy processes play an important role in the formation of inverse spinels [18,19].

The importance of closing this knowledge gap regarding the structural and kinetic properties of this ferrite has motivated us to implement computational tools and methods that allow us to contribute to the understanding of these processes at the atomic scale.

More specifically, in this work we combine experimental evidence on the formation of the inverse spinel of $NiFe_2O_4$ with a computational study of atomistic diffusion using the k-ART algorithm to understand the mechanisms responsible for the transition from normal to inverse spinel.

2. Experimental and computational procedure

2.1. Synthesis and characterization of $NiFe_2O_4$ inverse spinel

$NiFe_2O_4$ ferrite was synthetized by solid state reaction. The initial oxides α-Fe_2O_3 and NiO were premixed manually in an agate mortar for 30 min in order to homogenize. Then a mechanical mixing was carried out in a Fritsch Pulverisette 5 planetary ball mill. The resulting mixture was calcined in air at 1150∘C for 12h. Then the samples were highly densified by a sintering process at 1300 °C for 24 h. The structural analysis of the samples was performed by X-ray diffraction (XRD), using a Panalytical Empyrean series 2 (CuKα 1.5405 Å). In addition, ^{57}Fe Mössbauer spectra were recorded on a conventional spectrometer using a ^{57}Co(Rh) radioactive source at room temperature in transmission geometry, and their hyperfine parameters (hyperfine field, quadrupole and isomeric shift values) were obtained using the Recoil program. Finally, all spectra were fitted using the standard α-Fe absorber as a calibration.

2.2. Computational procedure

For simplicity in this study, we have only considered the analysis of diffusion in a normal spinel box of 2×2×2 unitary cells, for a total of 448 atoms, where Ni^{2+} and Fe^{3+} fill A and B sites respectively, required to account for the effects produced by the stress associated with defects. Other properties of a perfect spinel crystal such as geometry, elastic constants, shear modulus, cohesive and vacancy formation energies were previously discussed in ref. [20].

Diffusion coefficients and migration energies are usually investigated with molecular dynamics (MD). By plotting diffusion over a range of temperatures, it is possible to extract effective diffusion energy barriers using Arrhenius plots. Further analysis is required, however, with this approach to extract atomistic mechanisms. Moreover, because of the time scale limits of this method, it is not always possible to access all relevant mechanisms of diffusion, especially when barriers are high with respect to the temperature available to MD. To overcome these limitations, we use kinetic Monte-Carlo (KMC) code k-ART, an off-lattice on-the-fly algorithm with topological classification which has been developed to explore the energy landscape and long-time kinetics of complex systems at the atomic scale. K-ART fully includes long-range elastic events and disordered environments [21–23], providing detailed atomic description of activated events. These events represent the main states in the transition from one local energy minimum to another minimum in the configurational space that is connected by a single transition state. Thus, an event can be reduced to three atomic configurations: initial minimum, final minimum and the connecting saddle point. To simplify storage (3*N* atoms per event), k-ART uses a topological characterization of the local environment surrounding each atom to classify these configurations. K-ART also uses the basin-auto constructing mean rate method (bac-MRM) to address the critical slowing down of kinetic Monte Carlo simulations caused by flickering states, states of similar energy separated by low-energy barriers that can slow system evolution to a halt [23,24].

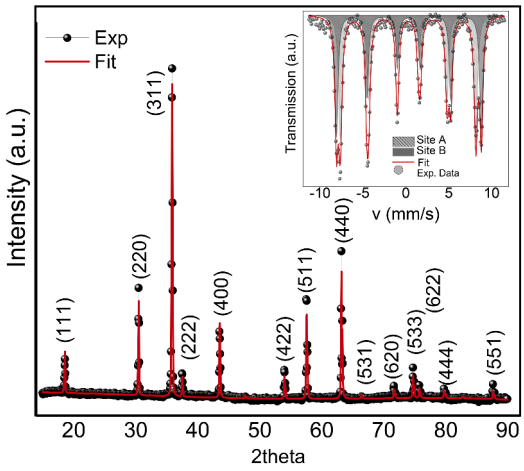

Fig. 1. XRD pattern for bulk $NiFe_2O_4$ sample prepared by solid state reaction. Continuous line is the fit by Rietveld refinement and solid sphere are experimental data. Inset: experimental and fitted room temperature Mössbauer spectra for $NiFe_2O_4$.

The square displacement is computed according to $SD(t_n) = \sum_{i=1}^{N}(\boldsymbol{x}_i(t_n) - \boldsymbol{x}_i(0))^2$, where N is the number of particles and $\boldsymbol{x}_i(t_n)$ is the position of atom i at KMC step n and time t_n. The diffusion coefficient over a total of M steps is computed using Einstein's formula $D = \left(\frac{1}{6t_M^2}\right)\sum_{n=1}^{M} SD(t_n)\Delta t_n$, where a time average is considered according to the ergodic hypothesis. We use the k-ART coupled with the Buckingham potentials [25]. The implementation is done by constructing tabulated potentials for the LAMMPS library package [26,27], which is used as the force-calculation engine and which is linked to our k-ART code. The potential correctly predicts the geometry at zero pressure, with a lattice constant of 8.606 Å, whereas the experimental value is 8.339 Å. The predicted bulk modulus is 164.57 GPa while the experimental value is 198.2 GPa [25,28].

3. Results and discussion

The crystal structure of bulk $NiFe_2O_4$ is revealed by XRD analysis. Structure parameters are determined by Rietveld refinement (JCSD reference code: 98-004-0040) on data diffraction patterns. The experimental XRD pattern and theoretical XRD curve, as obtained after Rietveld refinement for $NiFe_2O_4$ are presented in Supplementary Figure S1. The result indicates a single phase corresponding to $NiFe_2O_4$ with a lattice parameter of 8.3385(3) Å (see Supplementary Table 1) with *Fd-3m* symmetry in agreement with Ref. [14]. Each observed reflection is indexed as shown in Fig. 1. To gain further insight into the iron distribution in the spinel structure, a Mössbauer study was performed on the $NiFe_2O_4$ sample at room temperature. The inset in Fig. 1 shows the Mössbauer spectra (MS) with the corresponding fitting model used for

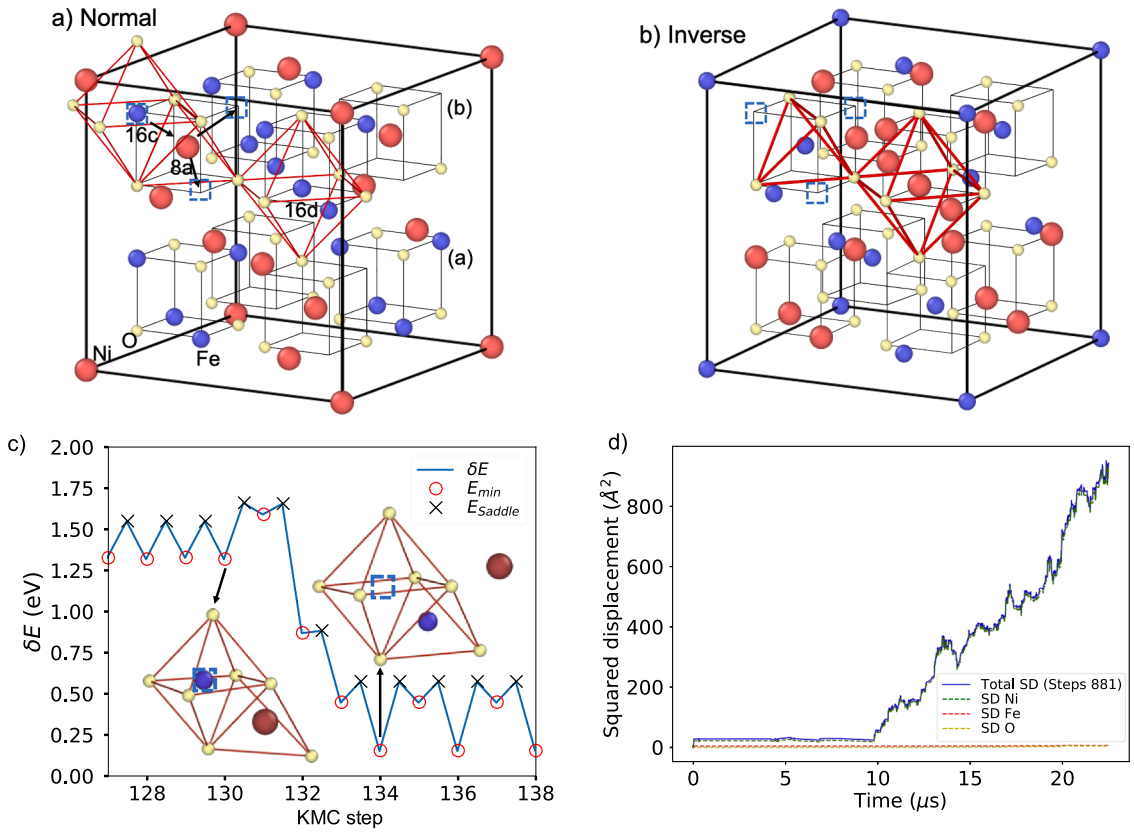

Fig. 2. Normal (a) and inverse (b) phases of an ideal spinel; dotted squares are 16c interstitial sites and arrows indicate jump directions. In (c) the triggering energies involved for Ni ion diffusion. Insets: the interstitial Fe takes the Ni place stabilizing at the tetrahedral site and Ni starts diffusing. In (d) squared displacement *SD* of Fe, Ni and O ions.

the experimental data, which is in agreement with the results of Ref. [7]. The spectra are well fitted by two magnetic sextets associated to site A (light gray) and B (dark gray) of the iron of the nickel-ferrite compound. In accordance with hyperfine parameter values for $NiFe_2O_4$ sample relative to the α-Fe, the first component is related to Fe^{3+} cations in tetrahedral sites with hyperfine parameters values of isomer shifts (IS) of 0.25 mm/s, quadrupole splitting (QS) of 0.01mm/s, hyperfine magnetic field (Heff) of 49.1 Tesla and normalized site population (A%) of 51.1 %. The second component corresponds to Fe^{3+} cations in octahedral sites with IS = 0.36mm/s, QS = 0.0 mm/s, Heff = 52.4 Tesla and B% = 48.9 %. The ratio of the spectrum areas corresponding to A and B sites in the $NiFe_2O_4$ structure is A/B = 1.02, which corresponds to an inverse spinel.

The above results suggest that a nickel ferrite inverse spinel can be obtained by a solid state reaction. However, since these experimental techniques can only identify the spinel type and the location of the iron ions in the A and B sites, they are not sufficient to describe how this process occurs during synthesis. For this, simulations are necessary.

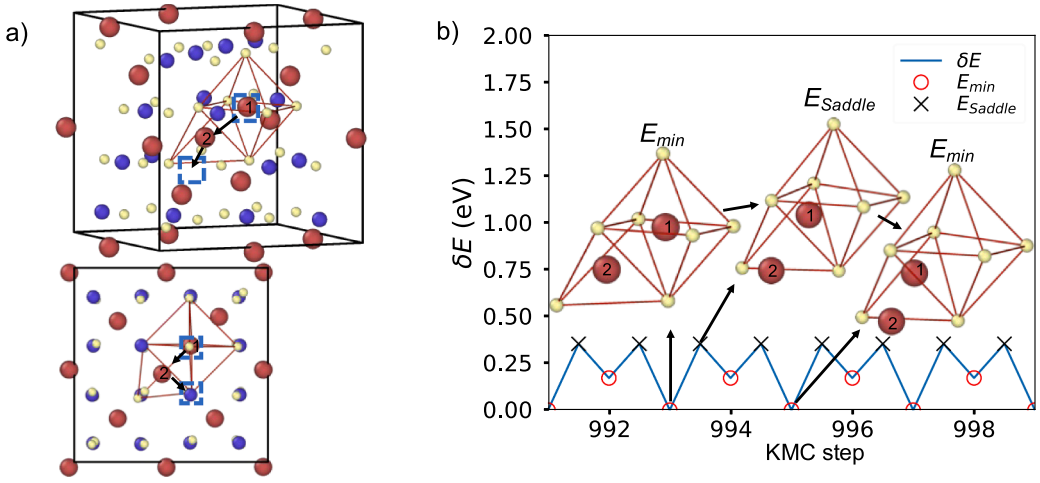

Fig. 3. Ni-interstitial diffusion mechanism. In a), unit cell 3D (displaced by half lattice in each direction) and top view along the (100)-direction. The red, blue and yellow spheres correspond to Ni, Fe and O atoms, respectively. The red spheres numbered 1 and 2 represent the diffusing Ni1 and Ni2 ions. In b) the change in energy δE when jumping from one minimum to another via saddle point as shown in the Insets.

3.1. Interstitial diffusion mechanisms of cations

For simplicity, all simulations start with a normal spinel system relaxed to zero pressure prior to the KMC steps. A normal spinel can be represented as an fcc cubic cell with eight cubic octants of type (a) and (b) as shown in Fig. 2a. The possible symmetric interstitial points involved in diffusion in a normal spinel cell are also shown in the inset of Fig. 2a, they are: tetrahedral 8a, octahedral 16c and 16d. Points 16d belong to cornets of (a) octants and points 16c belong to corners of (b) octants. The 16c octahedral site shares faces with the 8a tetrahedral site and the 48f tetrahedral site (not shown because it does not participate in diffusion here, but the 48f site shares faces with the 16c and 16d sites) [5]. Then, an interstitial Ni/Fe ion is initially randomly located, but after relaxation it occupies a 16c site. For comparison, Fig. 2b shows an ideal inverse spinel unit cell.

Simulations are done at 300 K. The Fe-interstitial diffusion is not observed, rather we find one of the most surprising mechanisms in spinel diffusion: it is the one by which a Fe-interstitial triggers Ni diffusion. More precisely, after the Fe-interstitial relaxing to an octahedral 16c site, by series of steps it jumps to a tetrahedral 8a site occupied by Ni, thus displacing Ni ion to an interstitial 16c octahedral site and triggering Ni diffusion. Fig. 2c describes this activation mechanism which occurs with a barrier of 0.34 eV at step 130 (activation of migration of Fe interstitial from octahedral to tetrahedral sites and migration of Ni to 16c site) and Ni diffusion after step 134 with barriers 0.18 and 0.35 eV. A total effective inverse barrier of ~1.5 eV, separates the initial and final states from steps 130 to 134. Also, is interesting to note that DFT calculations predict an energy preference of 1.5 eV for the inverse structure [19]; in our case, the difference between the minima at 130 and 134 is ~1.2 eV. This makes very difficult for the Ni ion to return to the tetrahedral site 8a as it is more energetically stable with Fe, thus transforming the normal to inverse spinel. Therefore, this mechanism explains how Fe-interstitials help to form inverse spinels, the most common $NiFe_2O_4$ spinel structure and why the normal spinel is never observed. The plots of the square displacement *SD* for the three ion types are shown in Fig. 2d, where it is observed that only Ni diffuses, as we will explain in the following paragraph.

In more detail, Fig. 3 describes the Ni-interstitial diffusion mechanism, which occurs in five steps involving two Ni ions, labeled as Ni1 and Ni2 shown in Fig. 3a. After the Ni1 interstitial relaxes to an octahedral site 16c, diffusion starts by the octahedral Ni1 displacing the Ni2 at the tetrahedral site 8a to an octahedral site 16c and taking its site, the cycle is repeated by the displaced Ni2 at the new 16c by displacing another Ni ion. The diffusion coefficient is $\sim 6.4 \times 10^{-14}$ m^2/s with barrier energies of 0.18, 0.35 eV and 0.47 eV. The two minima and saddle positions with respect to tetrahedral and octahedral sites are shown in Fig. 3b. It is also interesting to note the similarity of the diffusion mechanism of Ni with respect to that of Fe, as Ni at site 16c takes the place of a neighboring Ni ion at site 8a, a mechanism not expected by normal intuition and in contrast to intuitive mechanisms such as a jump from 16c to 16c via a tetrahedral site 48f, which is not chosen as the preferred path here. Comparing Figs. 2 and 3, we can conclude that the jumps are essentially the same for Ni and Fe ions, involving two ions per jump, but after the first jump only Ni diffuses, so Fe actually prefers to be at octahedral sites 8a.

These mechanisms clearly show the role of interstitial cation diffusion in the formation of the inverse spinel phase, since after nucleation, Fe and Ni interstitial diffusion mechanisms are fundamental for the final formation of the inverse spinel as predicted by our computational KMC studies here. Although, as explained above, several works have studied the distribution of transition metal ions between octahedral and tetrahedral sites in this type of spinel [6–8], none of them provides a satisfactory explanation of the inverse phase formation from an atomic point of view. The usual computational procedure to explain diffusion is to intuitively propose the initial and final minima states and then use DFT or classical empirical potentials to obtain the energy barrier separating these states [29,30,19]. However, this approach does not allow the elucidation of the mechanisms underlying the inverse and normal phase relations and the role of diffusion on them. Moreover, the elucidation of inverse spinel formation is not easily compressible from the experimental point of view, because spinel ferrites can be synthesized by different experimental methods and the physicochemical reactions are strongly dependent on them [31–36], thus the role of cation diffusion is hidden. However, the use of KMC simulations, as done here, has allowed us to understand how Fe interstitials do not allow normal spinel formation due to their preference for tetrahedral 8a sites and the low barrier required to jump onto them, removing Ni ions from these sites.

Although for simplicity we have assumed that the initial structure after nucleation is a normal spinel structure, this is not actually the experimental case. At high temperatures one would expect the spinel to tend towards a random cation arrangement rather than a normal one, i.e., it would be more likely that the spinel structure would be quenched to form an inverse spinel arrangement rather than a normal one. However, using a normal spinel has allowed us to understand why the inverse spinel, which is predicted to be stable, cannot form in the presence of interstitials.

In summary, it is shown that interstitial Fe ions can play a relevant role in the formation of inverse spinel, as opposed to normal spinel, after nucleation processes have occurred or during synthesis processes at some temperature, where Fe ions take the place of Ni ions thus triggering Ni diffusion and inverse spinel formation. Once the Fe ion displaces the Ni ion a large barrier of 1.50 eV is required for Fe diffusion, in contrast to the 0.35 eV barrier energy required for Ni diffusion. It was also found that the Ni diffusion path requires the exchange of two ions per step. Experimentally, the inverse spinel was corroborated by *ex situ* XRD and Mossbauer and measurements confirming the formation of an inverse spinel as expected.

Declaration of competing interest

The authors declare that they have no known competing financial interests or personal relationships that could have appeared to influence the work reported in this paper.

Acknowledgments

This work is supported in part by grants from the Natural Sciences and Engineering Research Council of Canada (NSERC). We are grateful to Calcul Québec/Compute Canada (CQ/CC) for generous allocations of computer resources. The k-ART package is available for distribution by contacting the authors. O. Arnache wants to thank for the financial support by Solid State Group - GES at the University of Antioquia in the framework of Sustainability Strategy 2020-2021, SIIU 2019-26150 project and by Colombian ministry of science and technology - Minciencias (project no. 111580863381, contract 325-2019 - Acta CODI-2019-25990).

Supplementary materials

Supplementary material associated with this article can be found, in the online version, at doi:10.1016/j.mtla.2024.102031.

References

[1] G.Y. Lai. High-temperature corrosion and materials applications, 2. print, ASM International, Materials Park, OH, 2008.
[2] G. Rekhila, Y. Bessekhouad, M. Trari, Visible light hydrogen production on the novel ferrite NiFe2O4, Int. J. Hydrog. Energy 38 (2013) 6335–6343.
[3] Ö.N. Avcı, L. Sementa, A. Fortunelli, Mechanisms of the oxygen evolution reaction on NiFe2O4 and CoFe2O4 inverse-spinel oxides, ACS Catal. 12 (2022) 9058–9073.
[4] D. Bacorisen, R. Smith, J.A. Ball, R.W. Grimes, B.P. Uberuaga, K.E. Sickafus, W. T. Rankin, Molecular dynamics modelling of radiation damage in normal, partly inverse and inverse spinels, Nucl. Instrum. Methods Phys. Res. B 250 (2006) 36–45.

[5] K.E. Sickafus, J.M. Wills, N.W. Grimes, Structure of spinel, J. Am. Ceram. Soc. 82 (2004) 3279–3292.
[6] J.M. Robertson, A.J. Pointon, The cation distribution in nickel ferrite, Solid State Commun. 4 (1966) 257–259.
[7] G.A. Sawatzky, F. Van Der Woude, A.H. Morrish, M"ossbauer study of several ferrimagnetic spinels, Phys. Rev. 187 (1969) 747–757.
[8] W.J. Tomlinson, J. Lilley, Kinetics of solid state NiFe2O4 formation at 700 to 1400° C, J. Mater. Sci. 13 (1978) 1148–1150.
[9] C.N. Chinnasamy, A. Narayanasamy, N. Ponpandian, K. Chattopadhyay, K. Shinoda, B. Jeyadevan, K. Tohji, K. Nakatsuka, T. Furubayashi, I. Nakatani, Mixed spinel structure in nanocrystalline NiFe2O4, Phys. Rev. B 63 (2001) 184108.
[10] R.H. Kodama, A.E. Berkowitz Jr., E.J. McNiff, S. Foner, Surface spin disorder in NiFe2O4 nanoparticles, Phys. Rev. Lett. 77 (1996) 394–397.
[11] G.D. Tang, D.H. Ji, Y.X. Yao, S.P. Liu, Z.Z. Li, W.H. Qi, Q.J. Han, X. Hou, D.L. Hou, Quantum-mechanical method for estimating ion distributions in spinel ferrites, Appl. Phys. Lett. 98 (2011) 072511.
[12] G.D. Tang, D.L. Hou, W. Chen, X. Zhao, W.H. Qi, Quantum-mechanical model for estimating the number ratio between different valence cations in multiatom compounds, Appl. Phys. Lett. 90 (2007) 144101.
[13] G.A. Kolta, S.Z. El-Tawil, A.A. Ibrahim, N.S. Felix, Kinetics and mechanism of zinc ferrite formation, Thermochimica Acta 36 (1980) 359–366.
[14] S.B. Narang, K. Pubby, Nickel spinel ferrites: a review, J. Magn. Magn. Mater. 519 (2021) 167163.
[15] S.C. Hendy, N.J. Laycock, M.P. Ryan, Atomistic modeling of cation transport in the passive film on iron and implications for models of growth kinetics, J. Electrochem. Soc. 152 (2005) B271.
[16] D. Carta, M.F. Casula, A. Falqui, D. Loche, G. Mountjoy, C. Sangregorio, A. Corrias, A structural and magnetic investigation of the inversion degree in ferrite nanocrystals MFe2O4 (M = Mn, Co, Ni), J. Phys. Chem. C 113 (2009) 8606–8615.
[17] C.M.B. Henderson, J.M. Charnock, D.A. Plant, Cation occupancies in Mg, Co, Ni, Zn, Al ferrite spinels: a multi-element EXAFS study, J. Phys.: Condens. Matter 19 (2007) 076214.
[18] A. Walsh, S.-H. Wei, Y. Yan, M.M. Al-Jassim, J.A. Turner, M. Woodhouse, B. A. Parkinson, Structural, magnetic, and electronic properties of the Co-Fe-Al oxide spinel system: density-functional theory calculations, Phys. Rev. B 76 (2007) 165119.
[19] C.L. Muhich, V.J. Aston, R.M. Trottier, A.W. Weimer, C.B. Musgrave, First-principles analysis of cation diffusion in mixed metal ferrite spinels, Chem. Mater. 28 (2016) 214–226.
[20] Ó.A. Restrepo, Ó. Arnache, J. Restrepo, C.S. Becquart, N. Mousseau, Comparison of bulk basic properties with different existing Ni-Fe-O empirical potentials for Fe3O4 and NiFe2O4 spinel ferrites, Comput. Mater. Sci. 213 (2022) 111653.
[21] N. Mousseau, L.K. Béland, P. Brommer, F. El-Mellouhi, J.-F. Joly, G.K. N'Tsouaglo, O. Restrepo, M. Trochet, Following atomistic kinetics on experimental timescales with the kinetic Activation–Relaxation Technique, Comput. Mater. Sci. 100 (2015) 111–123.
[22] F. El-Mellouhi, N. Mousseau, L.J. Lewis, Kinetic activation-relaxation technique: an off-lattice self-learning kinetic Monte Carlo algorithm, Phys. Rev. B 78 (2008) 153202.
[23] L.K. Béland, P. Brommer, F. El-Mellouhi, J.-F. Joly, N. Mousseau, Kinetic activation-relaxation technique, Phys. Rev. E 84 (2011) 046704.
[24] B. Puchala, M.L. Falk, K. Garikipati, An energy basin finding algorithm for kinetic Monte Carlo acceleration, J. Chem. Phys 132 (2010) 134104.
[25] W. Sun, J. Du, Interfacial structures of spinel crystals with borosilicate nuclear waste glasses from molecular dynamics simulations, J. Am. Ceram. Soc. 102 (2019) 4583–4601.
[26] S. Plimpton, Fast parallel algorithms for short-range molecular dynamics, J. Comput. Phys. 117 (1995) 1–19.
[27] LAMMPS, Molecular Dynamics Simulator. http://lammps.sandia.gov/index.html.
[28] Z. Li, E.S. Fisher, J.Z. Liu, M.V. Nevitt, Single-crystal elastic constants of Co-Al and Co-Fe spinels, J. Mater. Sci. 26 (1991) 2621–2624.
[29] G. Henkelman, B.P. Uberuaga, H. Jónsson, A climbing image nudged elastic band method for finding saddle points and minimum energy paths, J. Chem. Phys. 113 (2000) 9901–9904.
[30] B.P. Uberuaga, D. Bacorisen, R. Smith, J.A. Ball, R.W. Grimes, A.F. Voter, K. E. Sickafus, Defect kinetics in spinels: long-time simulations of MgAl2O4, MgGa2O4, and MgIn2O4, Phys. Rev. B 75 (2007) 104116.
[31] H. Salazar-Tamayo, K.E.G. Tellez, C.A.B. Meneses, Cation vacancies in NiFe2O4 during heat treatments at high temperatures: structural, morphological and magnetic characterization, Mat. Res. 22 (2019) e20190298.
[32] H. Salazar-Tamayo, K.E. García, C.A. Barrero, New method to calculate Mössbauer recoilless f-factors in NiFe2O4. Magnetic, morphological and structural properties, J. Magn. Magn. Mater. 471 (2019) 242–249.
[33] Z.Ž. Lazarević, Č. Jovalekić, A. Milutinović, D. Sekulić, V.N. Ivanovski, A. Rečnik, B. Cekić, N.Ž. Romčević, Nanodimensional spinel $NiFe_2O_4$ and $ZnFe_2O_4$ ferrites prepared by soft mechanochemical synthesis, J. Appl. Phys. 113 (2013) 187221.
[34] L.I. Granone, A.C. Ulpe, L. Robben, S. Klimke, M. Jahns, F. Renz, T.M. Gesing, T. Bredow, R. Dillert, D.W. Bahnemann, Effect of the degree of inversion on optical properties of spinel $ZnFe_2O_4$, Phys. Chem. Chem. Phys. 20 (2018) 28267–28278.
[35] R.C. Kambale, N.R. Adhate, B.K. Chougule, Y.D. Kolekar, Magnetic and dielectric properties of mixed spinel Ni–Zn ferrites synthesized by citrate–nitrate combustion method, J. Alloys Compd. 491 (2010) 372–377.
[36] W.J. Tomlinson, J. Lilley, Kinetics of solid state NiFe2O4 formation at 700 to 1400° C, J. Mater. Sci. 13 (1978) 1148–1150.